

Geophysical Research Letters[®]

RESEARCH LETTER

10.1029/2022GL099532

Special Section:

Results from Juno's Flyby of Ganymede

Key Points:

- Juno ultraviolet spectrograph mapped UV sunlight reflected by Ganymede's surface during the Juno orbit 34 Ganymede flyby
- The UV signature of pure water ice was detected in the north polar regions but not within other ice-rich regions including Tros crater
- Additional absorption features observed may be related to ammonia and ozone

Supporting Information:

Supporting Information may be found in the online version of this article.

Correspondence to:

P. M. Molyneux,
pmolyneux@swri.edu













Citation:

Molyneux, P. M., Greathouse, T. K., Gladstone, G. R., Versteeg, M. H., Hue, V., Kammer, J., et al. (2022). Ganymede's UV reflectance from Juno-UVS data. *Geophysical Research Letters*, 49, e2022GL099532. <https://doi.org/10.1029/2022GL099532>

Received 11 MAY 2022

Accepted 15 JUL 2022

Ganymede's UV Reflectance From Juno-UVS Data

P. M. Molyneux¹ , T. K. Greathouse¹ , G. R. Gladstone^{1,2} , M. H. Versteeg¹ , V. Hue¹ , J. Kammer¹ , M. W. Davis¹ , S. J. Bolton¹ , R. Giles¹ , J. E. P. Connerney³ , J. C. Gérard⁴ , and D. C. Grodent⁴ 

¹Southwest Research Institute, San Antonio, TX, USA, ²University of Texas at San Antonio, San Antonio, TX, USA, ³Space Research Corporation, Annapolis, MD, USA, ⁴Université de Liège, LPAP, STAR Institute, Liège, Belgium

Abstract During the Juno orbit 34 Ganymede encounter, the ultraviolet spectrograph mapped UV sunlight reflected by Ganymede from a closest approach altitude of 1,044 km, allowing us to study spatial variations in Ganymede's far ultraviolet reflectance at higher resolution than has previously been possible. We find that a characteristic signature of water ice seen around 165 nm in laboratory spectra is absent over much of the observed area, but is detectable in the north high latitude region. We suggest that the spectral difference between the high latitudes and other icy regions, such as Tros crater, may be explained by the presence of additional UV-absorbing contaminants such as NH₃ at lower latitudes. We also note a decrease in the relative reflectance of the high latitude regions at wavelengths >190 nm, which may be the start of a previously observed ozone absorption feature.

Plain Language Summary The ultraviolet spectrograph (UVS) instrument on the Juno spacecraft observed ultraviolet sunlight reflected by the surface of Jupiter's largest moon, Ganymede. Although we know from previous observations that Ganymede's surface contains a large amount of water ice, we found that Ganymede does not reflect ultraviolet light in the way we expected: while water ice is very reflective at ultraviolet wavelengths longer than 165 nm, Ganymede's surface does not reflect well at these wavelengths. The northern high latitudes were found to be more reflective than the low latitudes, suggesting that the polar regions are more water-ice rich than parts of the surface closer to the equator. The bright Tros crater, which is known to contain a large amount of water ice, had a low UV reflectance, which we suggest may be due to UV-absorbing material trapped within the ice there. These results will be useful for planning future investigations of Ganymede's surface composition by the UVS instrument on the upcoming JUICE mission, which will tour all three of Jupiter's icy moons before entering orbit around Ganymede.

1. Introduction

Jupiter's largest moon, Ganymede, has a surface composed primarily of water ice, as evidenced by its relatively bright (44%; Weiss, 2004) visible albedo and the presence of diagnostic H₂O absorption features in the near infrared (Kuiper, 1957; Moroz, 1965; Pilcher et al., 1972; Pollack et al., 1978). The distribution of H₂O varies across the surface: Ligier et al. (2019) find that the H₂O abundance may range from almost 60% in bright impact craters to ~10% near the apex of the trailing hemisphere. Large-scale trends are also apparent – early ground-based observations indicated that the leading hemisphere contains ~20% more ice than the trailing hemisphere (Pilcher et al., 1972), and at all longitudes there is a noticeable transition from darker terrain at near equatorial latitudes to bright, icy polar caps at latitudes >40° (Smith et al., 1979).

Ganymede's global surface variations may be related to varying degrees of bombardment by the Jovian magnetospheric plasma. Ganymede is tidally locked to Jupiter and has an orbital velocity less than that of the surrounding Jovian plasma, such that the same hemisphere – the orbital trailing hemisphere, centered at 270°W longitude – is always upstream relative to the plasma flow. However, the presence of Ganymede's mini magnetosphere (Kivelson et al., 1996) partially shields the trailing low latitudes from this particle flux, whereas the plasma is able to access the surface along open field lines in the polar regions, and via reconnection in the downstream/leading hemisphere low latitude regions (Khurana et al., 2007; Poppe et al., 2018). Sputtering of the surface by the impacting plasma, which may redistribute and brighten ice (via the introduction of light scattering defects), may therefore explain the observed spatial variations in albedo and H₂O IR absorption depth (e.g., Johnson, 1985, 1997; Khurana et al., 2007).

Although the presence of water ice on Ganymede is well established via visible and infrared observations, a surprising absence of a strong ultraviolet signature of H₂O has previously been noted at both Ganymede and Europa (Becker et al., 2018; Molyneux et al., 2020). Laboratory measurements show that the reflectance spectrum of water ice exhibits a sudden increase in reflectance at a wavelength of ~165 nm, appearing very dark at shorter wavelengths and highly reflective at longer wavelengths (Warren & Brandt, 2008). This sharp absorption edge is clear in reflectance spectra of Saturn's icy moons and rings (Bradley et al., 2010; Cuzzi et al., 2018; Hendrix et al., 2010, 2012, 2018; Hendrix & Hansen, 2008a; Royer & Hendrix, 2014; Wagener & Caldwell, 1988), even on the darker satellites like Phoebe (Hendrix & Hansen, 2008b), which has a visible albedo of ~6% and is therefore expected to contain relatively little H₂O on its surface. The exact wavelength of the increase in reflectance shifts to slightly longer wavelengths as the ice grain size increases, to a maximum of ~170 nm for ice grains with diameter >200 μm (Becker et al., 2018). However, observations by the Hubble Space Telescope (HST) Cosmic Origins Spectrograph show that the UV water edge is not detectable in disk-averaged reflectance spectra of either Ganymede's leading or trailing hemisphere (Molyneux et al., 2020). Instead of a sharp increase in reflectance at 165–170 nm as expected, both hemispheres gradually become more reflective with increasing wavelength in the 170–210 nm spectral region. Molyneux et al. (2020) find that this spectral shape may be expected if Ganymede's ice grains are contaminated with a small (<1% by mass) fraction of UV-absorbing material, but it is difficult to constrain the identity and origin of such contaminants without disk-resolved measurements to determine the distribution and investigate potential correlations with surface features or processes.

In this study, we present disk-resolved observations of Ganymede's sub-Jovian hemisphere by the Juno ultraviolet spectrograph (UVS) instrument during the Juno perijove (PJ) 34 Ganymede flyby. These new measurements allow us to investigate whether the UV H₂O absorption edge is equally suppressed at all longitudes and latitudes, or if regions of purer ice are present. The maps presented also demonstrate the potential for future surface composition investigations by the UVS instruments on the upcoming JUICE (ESA) and Europa Clipper (NASA) missions.

2. Observations

Ganymede was observed by Juno UVS during a close flyby on 7 June 2021, prior to PJ34. Between 16:52 and 17:04 UTC (spacecraft time) the instrument recorded emissions from Ganymede's auroral ovals, as well as reflected sunlight falling within its 68–210 nm bandpass (Gladstone et al., 2017). Juno's 2 RPM spin rate (Bolton et al., 2017) meant that the UVS field of view (FOV) scanned across Ganymede's disk once every 30 s. The UVS FOV fell partially or entirely on the sunlit hemisphere during 13 consecutive spins, starting at 16:57:55 UTC. When mapping the UV reflectance we consider only this sunlit data, obtained when the Juno-Ganymede distance (the distance from the spacecraft to the surface of Ganymede at the sub-Juno point) was between 1827 and 7,779 km. Observations of Ganymede's aurora during the PJ34 flyby, including dayside and nightside spins, are described elsewhere in this issue by Greathouse et al., 2022.

The Juno UVS FOV is a 7.2°-long slit divided into three sections: two 2.55° × 0.2° wide regions at either end and a narrow 2.0° × 0.025° slit in the middle (Greathouse et al., 2013). In this paper we consider only photons entering through the two wide portions of the slit, since the signal-to-noise ratio (SNR) in the narrow central section is considerably worse. The Juno spin rate results in short exposure times even in the wider portions of the slit, as the Juno UVS FOV moves by one slit width (0.2°) every ~17 ms. We therefore also rebin the data when mapping to improve the SNR, as discussed in the following sections. The number of counts per resolution element varies across the maps due to the changes in illumination and in the size of the UVS footprint on the surface. Representative count rate and SNR maps for a range of spatial bin sizes are provided in Supporting Information S1.

3. Results

3.1. UV Ratio Map

In order to determine which regions of Ganymede's surface are most likely to exhibit the spectral signature of water ice, we first binned the data into 2° bins in both longitude and latitude (equivalent to 92 × 92 km spatial resolution) to improve the SNR. For each spatial bin we calculated the ratio of photons detected in the wavelength range 190–210 nm (where H₂O appears bright) to photons in the range 150–170 nm (where H₂O appears darker). This ratio should be high in regions where significant ice is present, and low where the ice abundance is low.

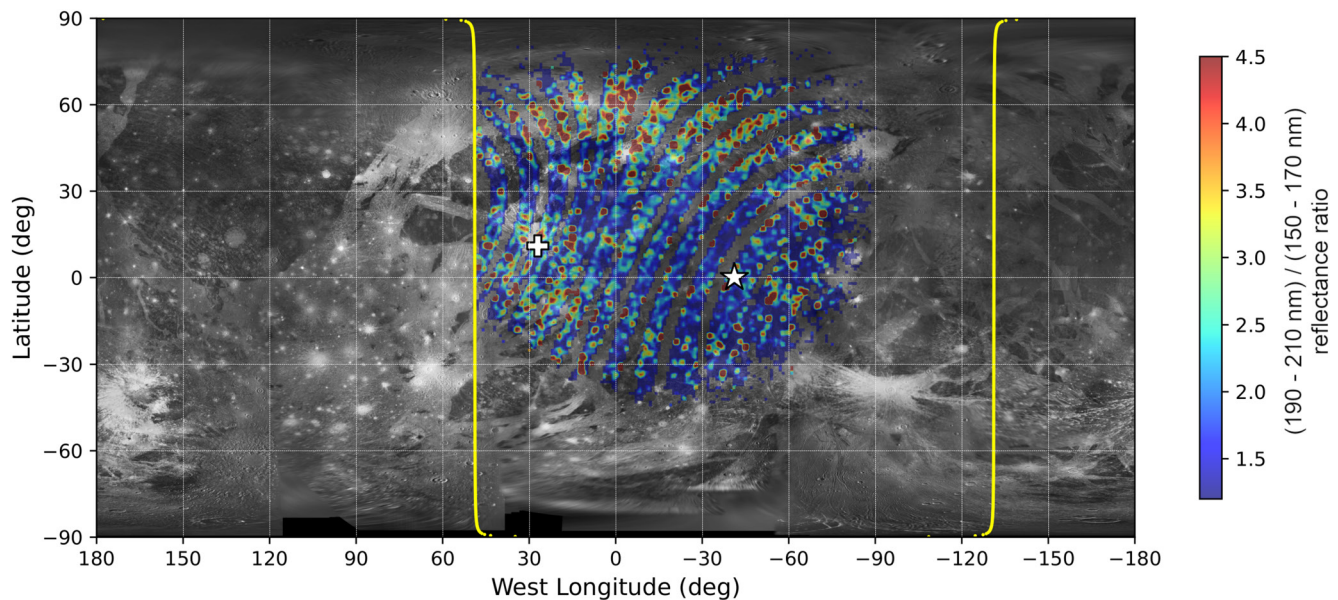


Figure 1. Map showing the ratio of reflected sunlight in two wavelength bands: 190–210 and 150–170 nm. Higher ratios imply higher H₂O abundance. The terminator and subsolar point are shown by the yellow line and white star. The location of Tros Crater is indicated by the white cross. (Ganymede map by Kersten et al., 2021).

(We note that the 150–170 nm band extends into the region of the ~165 nm increase in reflectance for small H₂O grains. However, shifting the wavelength band 5 nm shortward reduces the SNR of the map since the solar flux increases rapidly with increasing wavelength in this spectral region. Initial examination of Ganymede's reflectance as a function of latitude indicated that reflectance remains generally low until at least 170 nm – see Figure S1 in Supporting Information S1).

The UV reflectance ratio, R_{UV} , is determined based on the photon flux detected by UVS, F_{UVS} , in each of the two wavelength bands (band 1: 150–170 nm; band 2: 190–210 nm), and the solar flux, F_{sun} , in the same wavelength bands: $R_{UV} = [F_{UVS}(\text{band 2})/F_{sun}(\text{band 2})]/[F_{UVS}(\text{band 1})/F_{sun}(\text{band 1})]$. Since there is no instrument currently monitoring solar flux across the full Juno UVS wavelength range, we used the Naval Research Laboratory's Solar Spectral Irradiance (NRLSSI2) model solar spectrum (Coddington et al., 2016) for 2020.

Figure 1 shows a general trend of larger UV reflectance ratios at latitudes $>40^\circ$, coinciding with the location of the northern polar cap, and smaller reflectance ratios at low latitudes. The Juno UVS data also indicates that the region around the bright Tros crater (centered at 27°W , 11°N) is relatively icy compared to the surrounding low latitude terrain, as expected. No other significant correlations with crater locations or other specific surface features are apparent. The general distribution of ice according to this UV map is in good agreement with the distribution of a $2\ \mu\text{m}$ H₂O absorption feature mapped by Mura et al. (2020) using Juno JIRAM data from an earlier Juno flyby (orbit 24).

3.2. UV Reflectance Spectra

The short integration times of the Juno UVS exposures meant the SNR was too low to extract full spectra from each $2^\circ \times 2^\circ$ bin mapped in Figure 1. Instead, we extracted full UV spectra from three representative regions of Ganymede's surface, shown in Figure 2a: (a) a high latitude region where the reflectance ratio in Figure 1 was high; (b) a low latitude region where the reflectance ratio was low; and (c) the region around Tros crater. We divided each spectrum by the NRLSSI2 solar spectrum to obtain a reflectance spectrum for each region, and normalized each to their average reflectance in the 140–160 nm wavelength range. This normalization allows a direct comparison of the reflectance spectra without a full correction for the different sizes and viewing geometries of the three regions. The normalized spectra are shown in Figure 2b. We show only wavelengths >140 nm to exclude auroral oxygen emissions at 130.4 and 135.6 nm. The steep drop off in solar flux with decreasing wavelength in the FUV also reduces the reliability of results at wavelengths shortward of the oxygen emission lines.

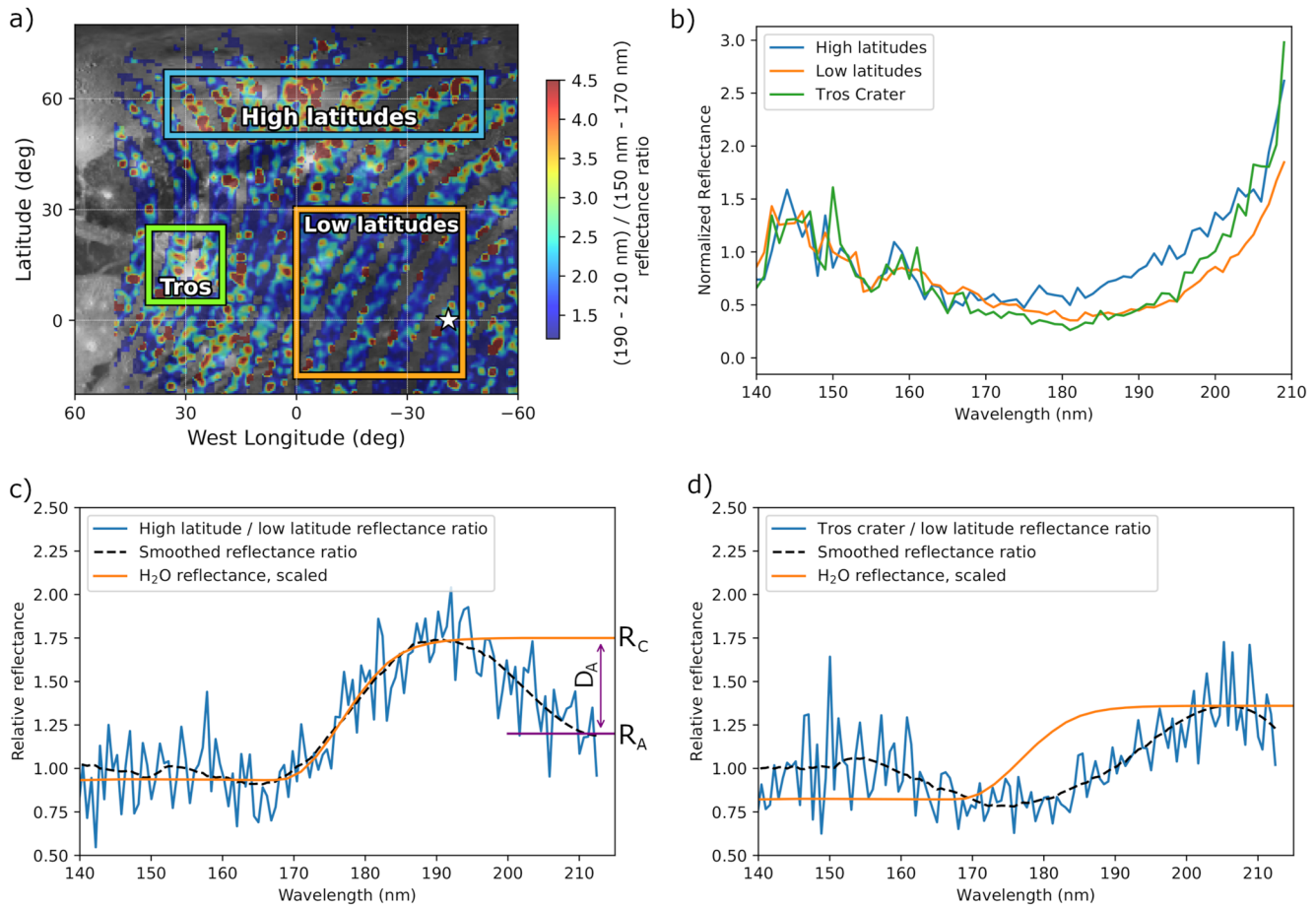


Figure 2. (a) Same as Figure 1, showing three regions used to extract reflectance spectra; (b) reflectance spectra for the three regions of interest, each normalized to the average reflectance in the 140–160 nm range; (c) ratio of the high latitude reflectance to the low latitude reflectance, with a modeled H₂O reflectance curve overplotted; (d) ratio of the Tros reflectance to the low latitude reflectance. The dashed lines in panels c and d show the reflectance ratio smoothed using a Savitzky-Golay filter with window length 51 (~30.6 nm) and polynomial order three, to guide the eye. Panel c is annotated to show the continuum and absorption reflectance values (R_C and R_A) used to calculate the depth of the ~210 nm absorption feature.

None of the reflectance spectra (Figure 2b) exhibit the sharp increase in reflectance at ~165 nm associated with H₂O, but there are slight differences between the reflectance of the three regions shown in Figure 2a. The low latitudes appear to be the least reflective region at $\lambda > 190$ nm, as expected, but whereas the high latitude spectrum starts to diverge from the low latitude spectrum at wavelengths > 160 nm, the region around Tros crater appears similar to the low latitudes up to 190 nm, increasing in brightness only at longer wavelengths than this.

To more clearly visualize the spectral differences in each region we divided both the high latitude spectrum and the Tros crater spectrum by the low latitude spectrum, as shown in Figures 2c and 2d. This technique of ratioing spectra to reveal masked spectral features has previously been used to detect ozone (Noll et al., 1996) and oxygen (Spencer et al., 1995) on Ganymede's surface. The UV H₂O feature that is not visible in the individual spectra becomes apparent in Figure 2c, indicating that the bright polar region contains more H₂O than the low latitudes, as expected. However, the same feature does not appear around Tros crater (Figure 2d) despite the known presence of ice there (e.g., Ligier et al., 2019; Mura et al., 2020). The modeled H₂O reflectance curves shown in Figure 2 were produced using the optical constants of Warren and Brandt (2008) and the Hapke bidirectional reflectance model (Hapke, 1981, 1984, 1986), assuming an H₂O grain size of 100 μm . The model is vertically scaled to match the approximate value of the Ganymede ratioed spectra at wavelengths either side of the expected position of the H₂O absorption edge.

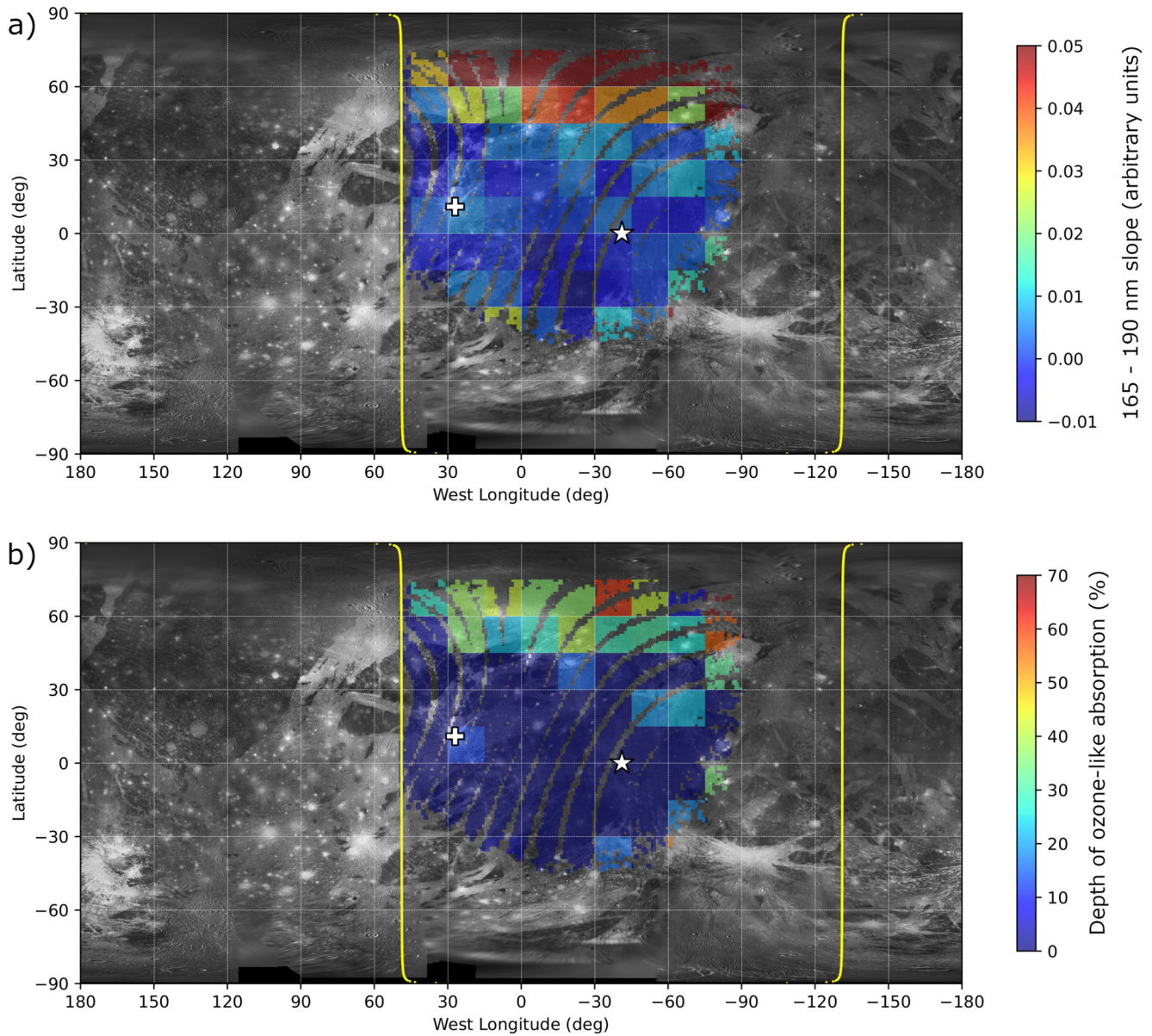


Figure 3. (a) Map showing the gradient at 165–190 nm in spectra extracted from $15^\circ \times 15^\circ$ bins across the observed region of Ganymede, relative to the average gradient at low latitudes. Larger values indicate a steeper slope, indicative of water ice. (b) Map of the depth of the >190 nm absorption feature averaged over $15^\circ \times 15^\circ$ bins.

3.3. Mapping of H₂O and Ozone-Like Spectral Features

To determine where on Ganymede's surface the UV ice feature is detectable, we produced normalized reflectance spectra as above across all surface regions observed by Juno UVS, averaged over $15^\circ \times 15^\circ$ bins. We then took the ratio of each extracted spectrum to that of the low latitude spectrum in Figure 2b to produce relative reflectance plots similar to Figures 2c and 2d. Finally, we performed a linear fit to the 165–190 nm region. The gradient of the best fit line is mapped in Figure 3a, with steeper gradients indicating a more confident detection of the H₂O absorption edge. The strongest evidence of water ice is seen at latitudes above 60°N. The increased ice concentration above 45°N is in good agreement with the location of the open/closed line field line boundary modeled by Khurana et al. (2007).

The relative reflectance plots shown in Figures 2c and 2d each start to decrease at long wavelengths, suggesting that Ganymede's brighter regions contain additional material that absorbs light at $\lambda > 190$ nm. This may be the

beginning of a broad ozone absorption feature previously observed at Ganymede in data from both HST and Galileo UVS, which peaks at 260 nm (Hendrix, Barth, & Hord, 1999; Noll et al., 1996). Figure 3b shows a map of the depth of the absorption feature, D_A , defined as $D_A = (R_C - R_A)/R_C$, where R_C is the reflectance of the continuum at the short wavelength edge of the absorption feature, and R_A is the minimum reflectance within the absorption band (see annotations in Figure 2c). When defining R_C and R_A , we used smoothed spectra similar to the dashed lines in Figures 2c and 2d, to minimize the influence of the scatter visible in the unsmoothed data. We took the maximum (R_C) and minimum (R_A) reflectance in the 180–210 nm region and visually inspected each spectrum to check that this method was not detecting any anomalous spectral features.

The absorption depth (Figure 3b) is greatest at high latitudes, which is consistent with the increased concentration of ozone in the polar regions measured by Hendrix, Barth, and Hord (1999), although there is little overlap between the spatial coverage of their observations and ours. However, we note that since the low latitudes appear darker than the high latitudes at $\lambda > 170$ nm, the observed distribution of this ozone-like absorption may be influenced by masking due to the presence of other UV-absorbing materials at low latitudes rather than evidence of a true spatial variation in ozone distribution.

Alternatively, the shape of the ratioed spectrum in Figure 2c may be interpreted as evidence of a material with a broad absorption peak around 190 nm at low latitudes rather than two absorbing materials (H_2O below 170 nm and O_3 above 190 nm) concentrated at high latitudes. We favor the interpretation requiring more H_2O at high latitudes due to the good agreement with the modeled position of the H_2O absorption edge and the consistency between the mapped H_2O distribution and that observed at infrared wavelengths, but as noted above it is possible that additional species at low latitudes also influence the spectral shape.

4. Discussion

The spectral differences we observed between Ganymede's high latitude regions and the area around Tros crater – both of which show clear evidence of water ice in the infrared – may result from differences in ice grain size and/or purity. Molyneux et al. (2020) present models of ice contaminated with minor species known or expected to exist at Ganymede including H_2O , silicates, and tholins (organic residue produced by irradiation of simple hydrocarbons) and show that, for a given contaminant concentration, the UV ice feature becomes more easily suppressed as the grain size is increased. Similarly, for a given ice grain size, the UV H_2O feature becomes less prominent as the contaminant concentration is increased. Therefore, our detection of H_2O in the north polar region but not near Tros or other optically bright craters observed by Juno UVS suggests that the polar ice is either less contaminated or consists of smaller grains.

Stephan et al. (2020) used band depth ratios from Galileo NIMS observations of Ganymede to constrain ice grain size as a function of latitude, and found that the grains are largest (~ 1 mm diameter) near the equator and smallest (as small as ~ 1 μm diameter) near the poles. At 50° – 67°N (the high latitude region in Figure 2a), and 11°N (Tros crater), the expected grain sizes are 10–200 μm and ~ 1 mm, respectively. Juno JIRAM results from an earlier Ganymede encounter (Juno orbit 24) also suggests an increased concentration of large ice grains around Tros crater compared to the surrounding terrain (Mura et al., 2020).

Higher sputtering rates are predicted to lead to larger average grain sizes due to preferential destruction of small grains (Cassidy et al., 2013; Clark et al., 1983), yet Ganymede's smallest grain sizes are observed in the high latitudes where sputtering rates are highest (Poppe et al., 2018). It is therefore likely that the grain size distribution observed on Ganymede is more strongly influenced by thermal effects, including annealing at the warmer low latitudes and thermal migration of H_2O vapor to the colder high latitudes (Johnson, 1997; Stephan et al., 2020), than by charged particle irradiation. However, Poppe et al. (2018) show that heavy ions (O^+ , O^{++} , S^{+++}) are able to access Ganymede's surface at low latitudes and may contribute to the accumulation of contaminants such as SO_2 and H_2O_2 there. Therefore, latitudinal variations in either grain size or contaminant concentration may explain the observed spectral differences at Ganymede.

We attempted to fit the Tros/low latitude ratioed spectrum shown in Figure 2d with a range of materials with known absorption features in the 140–210 nm region, including SO_2 , O_2 , CO_2 , C_6H_6 , and NH_3 . Each of these materials has been previously detected or suggested to exist at Ganymede (see Table S1 in Supporting Information S1 for a summary of Ganymede surface materials and references describing their detection). Modeled reflectance curves for the five materials are shown in Figure 4; the models were produced using absorption spectra

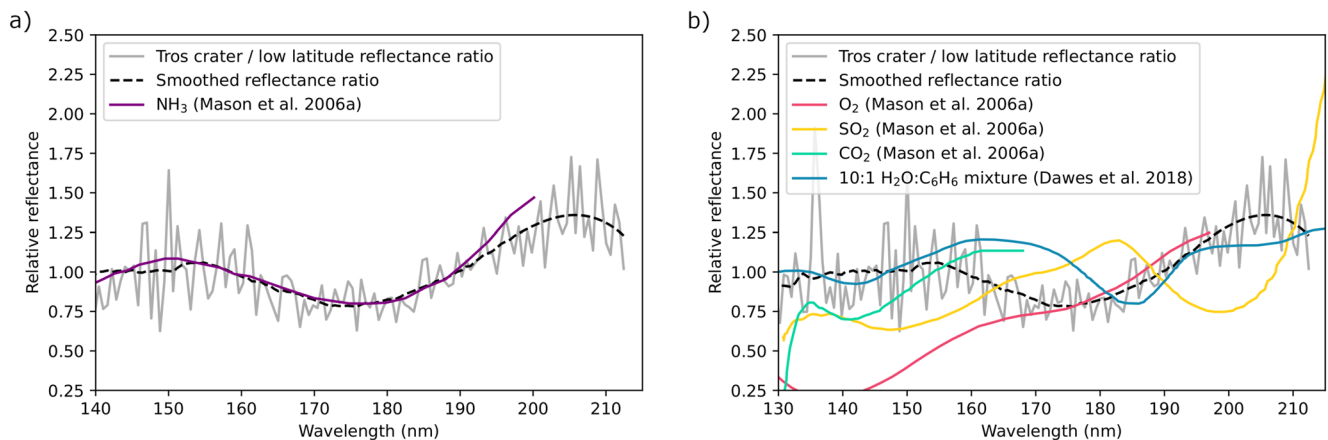


Figure 4. (a) Same as Figure 2d, with an inverted, scaled absorption spectrum of NH₃ overplotted; (b) Similar inverted, scaled absorption spectra of other UV-absorbing volatiles (O₂, SO₂, CO₂, C₆H₆) do not produce a good fit to the Tros crater/low latitude ratioed spectrum.

measured by Mason et al. (2006a) and Dawes et al. (2018), which we inverted and scaled so that the depth of the absorption feature closest to 180 nm matched the depth of the ~180 nm absorption feature in the Ganymede spectrum. Ammonia (NH₃) ice produced the best fit by far in terms of both the position and width of the expected absorption feature (Figure 4a).

Pure crystalline NH₃ ice exhibits a narrow absorption peak at 194 nm due to an exciton transition in the crystal (Mason et al., 2006a); its absence in the Tros spectrum is therefore more consistent with amorphous NH₃ or NH₃ within H₂O grains (Mason et al., 2006b) rather than crystalline ammonia ice. Further work is required to determine the concentration of NH₃ required to suppress the H₂O feature, to assess whether this concentration would produce detectable features at other wavelengths, and to investigate whether other bright craters also appear enriched in NH₃. We note that Mura et al. (2020) suggest that an absorption feature at 2.91 μm observed by JIRAM during the Juno PJ24 Ganymede encounter may be related to NH₃ ice, but since this is a weak feature falling within an intense water ice OH absorption band the identification is very tentative. Although NH₃ is commonly included in models of Ganymede's subsurface ocean, its possible detection in the ice at Tros is somewhat surprising as NH₃ • H₂O is volatile and dissociates under solar ultraviolet or charged particle irradiation (Brown et al., 1988).

Evidence of surface volatiles in Juno UVS spectra of Ganymede is an encouraging result from the perspective of the JUICE UVS instrument on the upcoming ESA JUICE mission (Grasset et al., 2013), which will end its tour of Jupiter's icy moons by entering a 500 km altitude orbit around Ganymede. The JUICE UVS bandpass of 50–204 nm (Davis et al., 2020) encompasses the H₂O and NH₃ absorption features as well as the beginning of the possible O₃ feature at λ > 190 nm. JUICE UVS should therefore be able to map the absorption features discussed in this paper almost as well as Juno UVS in terms of wavelength coverage, but with better spatial resolution and coverage, and with considerably longer integration times to increase SNR. In combination with observations of Ganymede's magnetosphere and atmosphere by the JUICE in situ instruments, the improved UV maps should allow the identity and origin of absorption features to be further constrained, and any diurnal variations (suggested by Hendrix, Barth, and Hord (1999) in their analysis of the 260 nm ozone absorption) to be investigated.

5. Conclusions

Juno UVS observed far ultraviolet sunlight reflected by Ganymede's sub-Jovian hemisphere, producing disk-resolved maps that allow the distribution of surface volatiles to be investigated. A characteristic UV signature of water ice was not present in reflectance spectra extracted from representative surface regions, including at high latitudes (>40°N) and around Tros crater, despite the known presence of significant ice in these regions (e.g., Ligier et al., 2019; Mura et al., 2020). However, by ratioing reflectance spectra of the icier regions to the low latitude average reflectance we were able to identify subtle spectral differences, and the UV ice feature became apparent at high latitudes only. This suggests that the high latitudes are enriched in pure ice relative to the low latitudes. The absence of the H₂O absorption edge in the Tros/low latitude ratioed spectrum may be explained by

the presence of an additional UV-absorbing contaminant – possibly ammonia – within the ice at Tros. We also observed a relative decrease in reflectance at long (>190 nm) wavelengths in the icy regions when compared to the reflectance at low latitudes, which may be the start of a previously observed broad absorption feature centered at 260 nm and attributed to ozone. The JUICE UVS instrument on the upcoming ESA JUICE mission will be capable of mapping both the water ice signature and the long wavelength absorption across the entirety of Ganymede's surface at higher spatial resolution and with longer exposure times than those achievable by Juno UVS, providing further insights into the origin and distribution of the UV-absorbing surface materials.

Data Availability Statement

Juno UVS data can be obtained from the Planetary Data System (PDS) at https://pds-atmospheres.nmsu.edu/data_and_services/atmospheres_data/JUNO/uvs.html. The calibrated data (Trantham, 2014) used in this study is located at https://pds-atmospheres.nmsu.edu/cgi-bin/getdir.pl?dir=DATA%26volume=jnouvs_3001. The NRLSSI2 solar spectrum can be obtained from the LASP Interactive Solar Irradiance Datacenter (LISIRD): https://lasp.colorado.edu/lisird/data/nrl2_ssi_P1Y/.

References

- Becker, T. M., Retherford, K. D., Roth, L., Hendrix, A. R., McGrath, M. A., & Saur, J. (2018). The far-UV albedo of Europa from HST observations. *Journal of Geophysical Research*, 123(5), 1327–1342. <https://doi.org/10.1029/2018je005570>
- Bolton, S. J., Lunine, J., Stevenson, D., Connerney, J. E. P., Levin, S., Owen, T. C., et al. (2017). The Juno mission. *Space Science Reviews*, 213(1), 5–37. <https://doi.org/10.1007/s11214-017-0429-6>
- Bradley, E. T., Colwell, J. E., Esposito, L. W., Cuzzi, J. N., Tollerud, H., & Chambers, L. (2010). Far ultraviolet spectral properties of Saturn's rings from Cassini UVIS. *Icarus*, 206(2), 458–466. <https://doi.org/10.1016/j.icarus.2009.12.021>
- Brown, R. H., Cruikshank, D. P., Tokunaga, A. T., Smith, R. G., & Clark, R. N. (1988). Search for volatiles on icy satellites. 1. Europa. *Icarus*, 74(2), 262–271. [https://doi.org/10.1016/0019-1035\(88\)90041-3](https://doi.org/10.1016/0019-1035(88)90041-3)
- Cassidy, T. A., Paranicas, C. P., Shirley, J. H., Dalton, J. B., Teolis, B. D., Johnson, R. E., et al. (2013). Magnetospheric ion sputtering and water ice grain size at Europa. *Planetary and Space Science*, 77, 64–73. <https://doi.org/10.1016/j.pss.2012.07.008>
- Clark, R. N., Fanale, F. P., & Zent, A. P. (1983). Frost grain size metamorphism: Implications for remote sensing of planetary surfaces. *Icarus*, 55(2), 233–245. [https://doi.org/10.1016/0019-1035\(83\)90036-2](https://doi.org/10.1016/0019-1035(83)90036-2)
- Coddington, O., Lean, J. L., Pilewskie, P., Snow, M., & Lindholm, D. (2016). A solar irradiance climate data record. *Bulletin of the American Meteorological Society*, 97(7), 1265–1282. <https://doi.org/10.1175/BAMS-D-14-00265.1>
- Cuzzi, J. N., French, R. G., Hendrix, A. R., Olson, D. M., Roush, T., & Vahidinia, S. (2018). HST-STIS spectra and the redness of Saturn's rings. *Icarus*, 209, 363–388. <https://doi.org/10.1016/j.icarus.2018.02.025>
- Davis, M. W., Gladstone, G. R., Giles, R. S., Greathouse, T. K., Molyneux, P. M., Raut, U., et al. (2020). Ground calibration results of the JUICE ultraviolet spectrograph. *Proceedings of SPIE*, 11444. <https://doi.org/10.1117/12.2562986>
- Dawes, A., Pascual, N., Mason, N. J., Gärtner, S., Hoffman, S. V., & Jones, N. C. (2018). Probing the interaction between solid benzene and water using vacuum ultraviolet and infrared spectroscopy. *Physical Chemistry Chemical Physics*, 20(22), 15273–15287. <https://doi.org/10.1039/c8cp01228h>
- Gladstone, G. R., Persyn, S. C., Eterno, J. S., Walther, B. C., Slater, D. C., Davis, M. W., et al. (2017). The ultraviolet spectrograph on NASA's Juno mission. *Space Science Reviews*, 213(1–4), 447–473. <https://doi.org/10.1007/s11214-014-0040-z>
- Grasset, O., Dougherty, M. K., Coustenis, A., Bunce, E. J., Erd, C., Titov, D., et al. (2013). Jupiter ICy moons Explorer (JUICE): An ESA mission to orbit Ganymede and to characterise the Jupiter system. *Planetary and Space Science*, 78, 1–21. <https://doi.org/10.1016/j.pss.2012.12.002>
- Greathouse, T. K., Gladstone, G. R., Davis, M. W., Slater, D. C., Versteeg, M. H., Persson, K. B., et al. (2013). Performance results from in-flight commissioning of the Juno ultraviolet spectrograph (Juno-UVS). *Proceedings of SPIE*, 8859. <https://doi.org/10.1117/12.2024537>
- Greathouse, T. K., Gladstone, G. R., Molyneux, P. M., Versteeg, M. H., Hue, V., Kammer, J., et al. (2022). UVS observations of Ganymede's aurora during Juno orbits 34 and 35. *Geophysical Research Letters*, 49, e2022GL099794. <https://doi.org/10.1029/2022GL099794>
- Hapke, B. (1981). Bidirectional reflectance spectroscopy. 1. Theory. *Journal of Geophysical Research*, 86(B4), 3039–3054. <https://doi.org/10.1029/jb086ib04p03039>
- Hapke, B. (1984). Bidirectional reflectance spectroscopy. 3. Correction for macroscopic roughness. *Icarus*, 59(1), 41–59. [https://doi.org/10.1016/0019-1035\(84\)90054-x](https://doi.org/10.1016/0019-1035(84)90054-x)
- Hapke, B. (1986). Bidirectional reflectance spectroscopy. 4. The extinction coefficient and the opposition effect. *Icarus*, 67(2), 264–280. [https://doi.org/10.1016/0019-1035\(86\)90108-9](https://doi.org/10.1016/0019-1035(86)90108-9)
- Hendrix, A. R., Barth, C. A., & Hord, C. W. (1999). Ganymede's ozone-like absorber: Observations by the Galileo ultraviolet spectrometer. *Journal of Geophysical Research*, 104(E6), 14169–14178. <https://doi.org/10.1029/1999je900001>
- Hendrix, A. R., Cassidy, T. A., Burratti, B. J., Paranicas, C., Hansen, C. J., Teolis, B., et al. (2012). Mimas' far-UV albedo: Spatial variations. *Icarus*, 220(2), 922–931. <https://doi.org/10.1016/j.icarus.2012.06.012>
- Hendrix, A. R., Filacchione, G., Paranicas, C., Schenk, P., Clark, R., & Scipioni, F. (2018). Icy Saturnian satellites: Disk-integrated UV-IR spectral characteristics and links to exogenic processes. *Icarus*, 200, 103–114. <https://doi.org/10.1016/j.icarus.2017.08.037>
- Hendrix, A. R., & Hansen, C. J. (2008a). The albedo dichotomy of Iapetus measured at UV wavelengths. *Icarus*, 193(2), 344–351. <https://doi.org/10.1016/j.icarus.2007.07.025>
- Hendrix, A. R., & Hansen, C. J. (2008b). Ultraviolet observations of Phoebe from the Cassini UVIS. *Icarus*, 193(2), 323–333. <https://doi.org/10.1016/j.icarus.2007.06.030>
- Hendrix, A. R., Hansen, C. J., & Holsclaw, G. M. (2010). The ultraviolet reflectance of Enceladus: Implications for surface composition. *Icarus*, 206(2), 608–617. <https://doi.org/10.1016/j.icarus.2009.11.007>
- Johnson, R. E. (1985). Polar frost formation on Ganymede. *Icarus*, 62(2), 344–347. [https://doi.org/10.1016/0019-1035\(85\)90130-7](https://doi.org/10.1016/0019-1035(85)90130-7)

Acknowledgments

This work was funded by NASA's New Frontiers Program for Juno via contract with the Southwest Research Institute.

- Johnson, R. E. (1997). Polar “caps” on Ganymede and Io revisited. *Icarus*, *128*(2), 469–471. <https://doi.org/10.1006/icar.1997.5746>
- Kersten, E., Zubarev, A. E., Roatsch, T., & Matz, K.-D. (2021). Controlled global Ganymede mosaic from voyager and Galileo images. *Planetary and Space Science*, *206*, 105310. <https://doi.org/10.1016/j.pss.2021.105310>
- Khurana, K. K., Pappalardo, R. T., Murphy, N., & Denk, T. (2007). The origin of Ganymede’s polar caps. *Icarus*, *191*(1), 193–202. <https://doi.org/10.1016/j.icarus.2007.04.022>
- Kivelson, M. G., Khurana, K. K., Russell, C. T., Walker, R. J., Warnecke, J., Coroniti, F. V., et al. (1996). Discovery of Ganymede’s magnetic field by the Galileo spacecraft. *Nature*, *384*(6609), 537–541. <https://doi.org/10.1038/384537a0>
- Kuiper, G. P. (1957). Infrared observations of planets and satellites. *The Astronomical Journal*, *62*, 245. <https://doi.org/10.1086/107539>
- Ligier, N., Paranicas, C., Carter, J., Poulet, F., Calvin, W. M., Nordheim, T. A., et al. (2019). Surface composition and properties of Ganymede: Updates from ground-based observations with the near-infrared imaging spectrometer SINFONI/VLT/ESO. *Icarus*, *333*, 496–515. <https://doi.org/10.1016/j.icarus.2019.06.013>
- Mason, N. J., Dawes, A., Holtom, P. D., Mukerji, R. J., Davis, M. P., Sivaraman, B., et al. (2006a). VUV spectroscopy and photo-processing of astrochemical ices: An experimental study. *Faraday Discussions*, *133*, 311–329. <https://doi.org/10.1039/b518088k>
- Mason, N. J., Dawes, A., Holtom, P. D., Mukerji, R. J., Davis, M. P., Sivaraman, B., et al. (2006b). VUV spectroscopy of extraterrestrial ices. *AIP Conference Proceedings*, *855*, 128.
- Molyneux, P. M., Nichols, J. D., Becker, T. M., Raut, U., & Retherford, K. D. (2020). Ganymede’s far-ultraviolet reflectance: Constraining impurities in the surface ice. *Journal of Geophysical Research: Planets*, *125*(9), e2020JE006476. <https://doi.org/10.1029/2020je006476>
- Moroz, V. I. J. A. Z. (1965). Infrared Spectrophotometry of the Moon and the Galilean Satellites of Jupiter. *Astronomicheskii Zhurnal*, *42*, 1287.
- Mura, A., Adriani, A., Sordini, R., Sindoni, G., Plainaki, C., Tosi, F., et al. (2020). Infrared observations of Ganymede from the Jovian InfraRed auroral mapper on Juno. *Journal of Geophysical Research: Planets*, *125*(12), e2020JE006508. <https://doi.org/10.1029/2020je006508>
- Noll, K. S., Johnson, R. E., Lane, A. L., Domingue, D. L., & Weaver, H. A. (1996). Detection of ozone on Ganymede. *Science*, *273*(5273), 341–343. <https://doi.org/10.1126/science.273.5273.341>
- Pilcher, C. B., Ridgway, S. T., & McCord, T. B. (1972). Galilean satellites: Identification of water frost. *Science*, *178*(4065), 1087–1089. <https://doi.org/10.1126/science.178.4065.1087>
- Pollack, J. B., Witteborn, F. C., Erickson, E. F., Strecker, D. W., Baldwin, B. J., & Bunch, T. E. (1978). Near-infrared spectra of the Galilean satellites: Observations and compositional implications. *Icarus*, *36*(3), 271–303. [https://doi.org/10.1016/0019-1035\(78\)90110-0](https://doi.org/10.1016/0019-1035(78)90110-0)
- Poppe, A. R., Fatemi, S., & Khurana, K. K. (2018). Thermal and energetic ion dynamics in Ganymede’s magnetosphere. *Journal of Geophysical Research: Space Physics*, *123*(6), 4614–4637. <https://doi.org/10.1029/2018ja025312>
- Royer, E. M., & Hendrix, A. R. (2014). First far-ultraviolet disk-integrated phase curve analysis of Mimas, Tethys, and Dione from the Cassini-UVIS data sets. *Icarus*, *242*, 158–171. <https://doi.org/10.1016/j.icarus.2014.07.026>
- Smith, B. A., Soderblom, L. A., Beebe, R., Boyce, J., Briggs, G., Carr, M., et al. (1979). The Galilean satellites and Jupiter: Voyager 2 imaging science results. *Science*, *206*(4421), 927–950. <https://doi.org/10.1126/science.206.4421.927>
- Spencer, J. R., Calvin, W. M., & Person, M. J. (1995). Charge-coupled device spectra of the Galilean satellites: Molecular oxygen on Ganymede. *Journal of Geophysical Research*, *100*(E9), 19049–19056. <https://doi.org/10.1029/95je01503>
- Stephan, K., Hibbitts, C. A., & Jaumann, R. (2020). H₂O-ice particle size variations across Ganymede’s and Callisto’s surface. *Icarus*, *337*, 113440. <https://doi.org/10.1016/j.icarus.2019.113440>
- Trantham, B. (2014). Juno J UVS reduced data record V1.0. In *NASA planetary data System*. <https://doi.org/10.17189/1518951>
- Wagener, R., & Caldwell, J. (1988). On the abundance of micron-sized particles in Saturn’s A and B rings. *ESA, A Decade of UV Astronomy with the IUE Satellite*, *1*, 85–88.
- Warren, S. G., & Brandt, R. E. (2008). Optical constants of ice from the ultraviolet to the microwave: A revised compilation. *Journal of Geophysical Research*, *113*(D14), D14220. <https://doi.org/10.1029/2007jd009744>
- Weiss, J. W. (2004). Appendix 2 – Planetary parameters. In F. Bagenal, T. Dowling, & W. B. McKinnon (Eds.), *Jupiter: The planet, satellites and magnetosphere, chapter 20* (pp. 699–706). Cambridge University Press.

References From the Supporting Information

- Domingue, D. L., Lane, A. L., & Beyer, R. A. (1998). IUE’s detection of tenuous SO₂ frost on Ganymede and its rapid time variability. *Geophysical Research Letters*, *25*(16), 3117–3120. <https://doi.org/10.1029/98gl02386>
- Hendrix, A. R., Barth, C. A., Stewart, A. I. F., Hord, C. W., & Lane, A. L. (1999). Hydrogen peroxide on the icy Galilean satellites. In *Lunar and planetary science conference abstracts*. 1540.
- McCord, T. B., Carlson, R. W., Smythe, W. D., Hansen, G. B., Clark, R. N., Hibbitts, C. A., et al. (1997). Organics and other molecules in the surfaces of Callisto and Ganymede. *Science*, *278*(5336), 271–275. <https://doi.org/10.1126/science.278.5336.271>
- McCord, T. B., Hansen, G. B., Clark, R. N., Martin, P. D., Hibbitts, C. A., Fanale, F. P., et al. (1998). Non-water-ice constituents in the surfaces of the icy Galilean satellites from the Galileo near-infrared mapping spectrometer investigation. *Journal of Geophysical Research*, *103*(E4), 8603–8626. <https://doi.org/10.1029/98je00788>
- Prockter, L. M., Head, J. W., Pappalardo, R. T., Senske, D. A., Neukum, G., Wagner, R., et al. (1998). Dark terrain on Ganymede: Geological mapping and interpretation of Galileo Regio at high resolution. *Icarus*, *135*(1), 317–344. <https://doi.org/10.1006/icar.1998.5981>
- Spencer, J. R. (1987). Icy Galilean satellite reflectance spectra: Less ice on Ganymede and Callisto? *Icarus*, *70*(1), 99–110. [https://doi.org/10.1016/0019-1035\(87\)90077-7](https://doi.org/10.1016/0019-1035(87)90077-7)